IOM 314.10 – 127

May 22, 1995

TO : Distribution

FROM : E M Standish, X X Newhall, J G Williams and W M Folkner

SUBJECT : JPL Planetary and Lunar Ephemerides, DE403/LE403

NOTE : The ephemerides DE403/LE403 replace DE402/LE402, for reasons explained in Standish (1995). Correspondingly, this memo replaces Standish *et al.* (1995).

I. INTRODUCTION

The latest JPL Planetary and Lunar Ephemerides, DE403/LE403, represent a number of recent improvements to previous ephemerides :

- • the ephemerides are now based upon the (J2000) reference frame of the International Earth Rotation Service (IERS),
- • the standard sets of observations have been augmented with more recent data,
- • a number of new data types have been added to the observational data set,
- • some of the data reduction techniques have been refined, and
- • the modeling of the perturbations of asteroids upon the planetary orbits has been improved.

The new reference frame is discussed in Section II; the observational data sets are described in Section III, along with plots of post-fit residuals for some of the data. Section IV discusses some of the recently improved reduction and modeling techniques; Section V compares DE403/LE403 with DE200/LE200, and Section VI gives tables of the initial conditions and dynamical constants of the integration.

II. IERS REFERENCE FRAME

In the past, the 1950-based ephemerides of JPL have been aligned onto the FK4 reference frame. Starting with DE200, attempts were made to align the ephemerides onto the dynamical equator and equinox of J2000 (see Standish, 1982). DE403, however, has been aligned onto the reference frame of the Radio Source Catalogue of the International Earth Rotation Service (IERS). This choice of reference frame is advantageous for a number of reasons.

- • The IAU-sponsored IERS is the organization which produces the timing and polar motion information used for the orientation of the earth. Since these data are referred to the IERS reference frame, there will automatically be consistency between the frame of the planetary ephemerides and the frame into which ground-based observatories and tracking stations are located. This assumes, of course, proper usage of the orientation data, including compatible values and models for precession, nutation, and pole offsets and the adoption of the IERS observatory and tracking station coordinates.
- • The JPL ephemerides are now fit to a number of observations which are referenced to the IERS Frame (see Section III); among all of the ephemeris observations which are explicitly given in a celestial reference system, these IERS-based ones are the most accurate.

- • The IERS Frame itself is accurate: the source positions are now determined at the sub-milliarcsecond level,
- • The IERS Frame is stable: an IAU directive to the IERS states that any further adjustments to the coordinates of the catalogue must be done in such a fashion that there is no net rotation introduced into the system as a whole
- • The IERS Frame is accessible and well-defined: the catalogue of source positions is published on an annual basis and is available worldwide.
- • Frame-ties between previous JPL ephemerides and the IERS Reference Frame have now been accurately ($\pm 0\farcs003$) determined (Folkner *et al.*, 1993).

A frame-tie between two ephemerides, in the present context, is defined by the alignments, at some specified date, of the earth's heliocentric position vector and the earth's heliocentric angular momentum vector.

Frame-ties between JPL (J2000) ephemerides created over the past decade or so show differences of up to $0\farcs1$. Fortuitously, however, the frame-tie between DE200 and the IERS reference frame, as determined by Folkner *et al.* (1993), is small:

$$\hat{\mathbf{r}}_{\rm IERS} \approx \hat{\mathbf{r}}_{\rm DE200} + \mathbf{A}(t) \times \hat{\mathbf{r}}_{\rm DE200} \quad \text{and} \quad \hat{\mathbf{h}}_{\rm IERS} \approx \hat{\mathbf{h}}_{\rm DE200} + \mathbf{A}(t) \times \hat{\mathbf{h}}_{\rm DE200}$$

where, for t = JED 2447435.5 (1 October 1988),

$$206265\ \mathbf{A}^T = [\ +0\farcs002 \pm 0\farcs002,\ +0\farcs012 \pm 0\farcs003,\ +0\farcs006 \pm 0\farcs003],$$

representing small rotations about the x-, y- and z-axes, respectively.

The vector $\mathbf{A}$ is time-dependent, but only slightly, due to the inaccuracies (about $0\farcs04$/cty) in the mean motion of the earth, most of which are in DE200. As the ephemerides have improved since that time, due to extended data, better values for the planetary masses, extended modeling of the asteroids' perturbations, etc., this time-dependence has decreased. Present-day uncertainties in the earth's mean motion are about $0\farcs015$/cty, due to the remaining uncertainties in the masses of the asteroids. As for orientation differences between future ephemerides, these should not differ from DE403 by any more than a few milliarcseconds, the uncertainties shown in the determination above.

Adjustment of DE403 onto the IERS Reference Frame

The frame-tie discussed above was treated as a (3rd rank) set of six observations, $\hat{\mathbf{r}}_{\rm IERS}$ and $\hat{\mathbf{h}}_{\rm IERS}$, to which the orbit of the earth in DE403 was adjusted. DE403 was also adjusted to fit the VLBI observations of Venus and Mars, discussed in the next section. These data serve to align the ephemerides onto the IERS frame and to improve the individual orbital elements, including the mean motions of the inner planets if the VLBI observations eventually span a decade or so. In addition, CCD measurements of the five outer planets and their satellites, in conjunction with CCD measurements of radio sources, may soon be used to refer those planets onto the IERS Frame.

III. OBSERVATIONAL DATA AND THEIR MODELING

Table I lists the observational data to which DE403/LE403 were adjusted. Many of the sets of observational data have been described before (Standish *et al.*, 1976; Standish, 1985, 1990); a number of these have been augmented by newer data.

The complete set of all of the data fit by the JPL ephemerides is kept by the authors along with a list of references to the sources.

Optical Observations

The sets of transit observations from Washington and the RGO (La Palma) have been extended; those from the RGO have included Pluto since 1989 (Morrison *et al.*, 1992). The sets from Bordeaux

and Tokyo have been added over the past few years. The collection of photographic observations of Pluto has been updated (Gemmo, 1994), and recent CCD observations of Pluto (Monet, 1994; Stone, 1995) have been added. Occultation timings from the rings of Uranus and from the disk of Neptune have been provided by Nicholson (1993).

However, all of the optical observations for the Sun, Mercury, Venus, and Mars were omitted from the least squares adjustment leading to DE403. Newer and more accurate data types (ranging, VLBI, etc.) determine these orbits far more accurately (by one or two orders of magnitude) than do the optical data. Since relatively large systematic errors are known to remain in the optical observations, and since there is a relatively large uncertainty connected with the frame-tie between the optical and IERS reference frames, the optical observations would possibly be detrimental for the inner planets.

For Jupiter, the ephemeris represents a compromise between inconsistent observations. As discussed in Standish (1995), "the orbital plane implied by the optical (FK5-based) observations disagrees with that implied by the IERS-based observations. The difference is about 0."2."

For the outermost four planets, the optical observations are crucial and are expected to remain so for a number of years. In addition to the standard transit observations, the timings of occultations of stars by the rings of Uranus and by the disk of Neptune provide supplementary information for those planets. Since these timings depend directly upon the position of the star being occulted, they are subject to all catalog errors: zone biases, proper motions, etc. Improved catalogues in the near future should greatly improve these observations.

Figures 1a–1h show right ascension residuals and declination residuals for the transit observations of the planets Jupiter through Neptune, and Figures 1i–1j show similar residuals for the photographic and (recent) transit and CCD observations of Pluto.

The transit observations from La Palma, Bordeaux and Tokyo were referenced to the FK5 system initially. The observations from Washington, dating back to the beginning of the century, were referenced to the Washington catalogue of the concurrent epoch; these were then transformed initially onto the FK4 reference system using the formulae of Schwan (1977). The transit observations from Herstmonceux and the astrolabe observations, as received, were referenced to the FK4 system. All optical observations which were initially referenced to the FK4 were then transformed onto the FK5 as described in the next paragraph.

In order to transform the FK4-based optical observations onto the FK5, corrections for general precession in longitude, $\Delta p = 1\overset{''}{.}10/\text{cty}$ and planetary precession, $\Delta\lambda = -0\overset{''}{.}029/\text{cty}$, (Fricke, 1971), and equinox offset and equinox motion, $E_0 = 0\overset{''}{.}525$ and $\dot{E}_0 = 1\overset{''}{.}275/\text{cty}$ (Fricke, 1982) were applied to the observations themselves. For the *apparent observed* values (transit and astrolabe observations), the standard corrections are

$$\alpha^O_{\rm FK5} = \alpha^O_{\rm FK4} + E_0 + \dot{E}_0\ T_{50}$$

and

$$\delta^O_{\rm FK5} = \delta^O_{\rm FK4},$$

where T_{50} is the time of the observation, expressed in Julian centuries past 1950.

For the *astrometric observed* values (photographic observations), the corrections are

$$\alpha^O_{\rm FK5} = \alpha^O_{\rm FK4} + E_0 - (\Delta k + \Delta n\ \sin\alpha\ \tan\delta)\ T_{50}$$

and

$$\delta^O_{\rm FK5} = \delta^O_{\rm FK4} - (\Delta n\ \cos\alpha)\ T_{50}$$

where ϵ is the obliquity of the ecliptic, and

where the standard notations, $\Delta k = -\dot{E}_0 + \Delta p\ \cos\epsilon - \Delta\lambda$ and $\Delta n = \Delta p\ \sin\epsilon$, are used.

For the *computed* values, both *apparent* and *astrometric*, the changes arise automatically when switching from computing with a B1950-based ephemeris using Newcomb's precession value to

computing with a J2000-based ephemeris using Fricke's precession value. These changes, for the *apparent* computed positions, are

$$\alpha^C_{\rm FK5} = \alpha^C_{\rm FK4} + E_0 + \dot{E}_0 + (\Delta k + \Delta n \ \sin\alpha \ \tan\delta) \ T_{50}$$

and

$$\delta^C_{\rm FK5} = \delta^C_{\rm FK4} + (\Delta n \ \cos\alpha) \ T_{50},$$

while the changes for the *astrometric* computed positions are

$$\alpha^C_{\rm FK5} = \alpha^C_{\rm FK4} + E_0 \quad \text{and} \quad \delta^C_{\rm FK5} = \delta^C_{\rm FK4}$$

Therefore, subtracting the above, it is seen that the residuals, (O–C), for both apparent and astrometric, become modified similarly:

$$(\alpha^O - \alpha^C)_{\rm FK5} - (\alpha^O - \alpha^C)_{\rm FK4} = -(\Delta k + \Delta n \ \sin\alpha \ \tan\delta) \ T_{50}$$

and

$$(\delta^O - \delta^C)_{\rm FK5} - (\delta^O - \delta^C)_{\rm FK4} = -(\Delta n \ \cos\alpha) \ T_{50}$$

Better determinations for the value of precession are now available from VLBI and Lunar Laser Ranging observations. Therefore, a further correction to the Fricke's IAU value for precession (Lieske *et al.*, 1977) was adopted into the least squares solution: $\Delta p \doteq -0\farcs3$/cty, in agreement with a number of recent determinations (Williams et al., 1994; Charlot et al., 1994; Souchay et al., 1995). With Δn (i.e., Δp) adopted, the adjustment of Δk absorbs any linear trend in the right ascension residuals; i.e., an adjustment to the combination of Fricke's value of the equinox motion and any other linear trend. The solution gave $\Delta k = -0\farcs208$/cty. For the obliquity rate, a correction of -0."024/cty was adopted to match the theoretical value of Williams (1994).

Since the optical observations are referenced to the FK5 frame, as modified by the corrections to precession and equinox drift, it becomes necessary to solve for a difference between the orientation of this frame and that of the IERS frame. This was done using a vector formulation similar to that described in Section II. However, it is necessary to have both optical and IERS-based observations of the same planet in order to determine the frame-tie. Since the optical observations of the inner planets are no longer included in the ephemeris adjustments and since there are very few IERS-based observations of the outer planets, the determination of the rotation vector should not be construed as a significant determination of the FK5-IERS frame-tie.

Signatures are still apparent in the optical data. These are probably due, in some part, to catalog zone errors and to errors in the original reduction processes. This is especially true for the Pluto observations where the data come from many and varied sources and are based almost entirely upon narrow field astrometry.

Viking Range Observations

Figures 2a–2c show the range residuals from the Viking Lander Spacecraft. It can be seen that observations clustered closely together within a single day tend to have a scatter of only 2–3 meters, thus giving an indication of the reproducibility of these measurements. However, the scatter from one day to another is 7–10 meters, probably the result of errors in the calibration of the transmitter-receiver hardware, errors in the (pre-launch) calibration of the transponder hardware (on the landers), or errors in using the dual-frequency signals from the orbiters (when available) to calibrate the time delay of the lander's signal caused by the interplanetary ionized electrons. The data have been analyzed further, testing whether the amount of scatter is correlated to the separation in time between the lander measurements and the calibration using the orbiter measurements. Nothing significant was found.

For the orientation of Mars, the spin-rate and the angles and rates relating the martian equator to the martian orbit were adjusted in the least-squares solution, as were the parameters describing the Mars centered coordinates of the two lander spacecraft (see, e.g., Standish, 1990). The nutation

model of Lyttleton *et al.* (1979) was used; this model shows adequate agreement with the models of Borderies (1980) and of Reasenberg and King (1979). Table II gives the results for the parameters, where the adjusted parameters are shown with their formal uncertainties. The values of the obliquity and its rate, ϵ and $\dot{\epsilon}$ come from Standish (1982); the values for $\Omega, \dot{\Omega}, I$, and $\dot{I}$, the angles and rates of the node and the inclination of the martian orbit upon the ecliptic, were determined by a fit to a previous ephemeris over the time of the Viking data.

Radar Observations

Radar-ranging observations of Mercury and Venus now exist through 1990 and of Mars through the 1992–93 opposition, taken by the Goldstone antennae. The residuals for Mercury and Venus are plotted in Figures 3a and 3b. The improvement in the scatter of the observations from the early days in the 1960's is evident. For Mercury, an elliptically shaped equator has been fit and removed from the residuals, using the form, $-c\Delta\tau = R_{\rm Mercury} + a\ \cos(2\lambda) + b\ \sin(2\lambda)$, where λ is the longitude of the echo point on the surface of Mercury, and where the fit gave $a = -2.20 \pm 0.26$ km and $b = -1.96 \pm 0.27$ km, and $R_{\rm Mercury} = 2439.93 \pm 0.05$ km.

For Venus, a topographical model of the surface, derived from Pioneer-Venus Orbiter data (Pettengill *et al.*, 1980), was used to reference the measurements to a sphere of radius 6052.26 ± 0.03 km, determined in the least squares adjustment. The high accuracy of these observations is due to the closeness of Venus at inferior conjunction and to the availability of the topographical model. As is seen, there have not been many measurements of Venus in the past decade or so. Certainly, more would be highly useful. Venus is relatively free from the asteroid perturbations that introduce uncertainties into the ephemeris of Mars, so that its ephemeris can be more accurately projected in time. Therefore, the Venus orbit, (which connects Venus into the inner planetary system), in conjunction with the VLBI observations of Venus, is important in orienting the inner planet system onto the radio frame. At present, five of the VLBI observations of Venus have been reduced (see below); another sixteen have been taken and are awaiting reduction (Folkner, 1995).

The 1992–93 Mars radar-ranging data can be used to assess the accuracy of the Mars ephemeris a decade after the highly accurate Viking Lander ranging data. Since the topography of Mars is extremely rough (20 km variations), only radar observations whose reflection points are near to each other on the surface of Mars can be meaningfully compared. For the 1992-93 opposition, the observations were at martian latitudes $+6\overset{\circ}{.}8$ and at $+8\overset{\circ}{.}5$. Only the observations from 1975-76 and 1978 oppositions are even reasonably close to these: $+4\overset{\circ}{.}3$ (and south) during 1975–76 and $+9\overset{\circ}{.}4$ (and north) during 1978. Consequently, the comparison of the 1992–93 data cannot give the 100-meter accuracy attained when the latitudes are within only 1° of each other (see, e.g., Standish *et al.*, 1976). Figures 4a–4c show the residuals for the individual echoes from the 1975–76, 1978 and 1992–93 oppositions, respectively, computed w.r.t. the 6-millibar surface (Christensen, 1979) and plotted versus longitude on Mars. The three oppositions are superimposed in Figure 4d which indicates that the ephemeris for Mars has no multi-kilometer drift over the past two decades and should be expected to maintain a similar accuracy into the future.

VLA Measurements of the Thermal Emission from the Jovian Planets and Their Satellites

Radio interferometry techniques have been used to measure the emitted flux from the Jovian and Saturnian satellites and from the disks of Uranus and Neptune (Muhleman *et al.*, 1985, 1986, 1988; Berge *et al.*, 1988). The center of the extended radio source may be determined to an accuracy of about $\pm 0\overset{''}{.}03$. Atmospheric refraction, however, possibly introduces further uncertainties into the declination component, especially if the radio catalogue sources used for calibration are relatively remote from the planet or satellite being observed. The effects of longitude errors in the satellite ephemerides were minimized by choosing observation times when the satellites were near maximum elongation from the planet.

VLBI and Radiometric Observations of Spacecraft

VLBI measurements of a spacecraft with respect to background sources from a radio source catalogue may be combined with the planetocentric spacecraft trajectory in order to yield a positional determination of the planet with respect to the reference frame of the radio source catalogue. A planet's position may also be determined using the more conventional range and doppler signatures in the radiometric spacecraft tracking data. The ephemeris adjustment for DE403 used both types of spacecraft measurements:

- • VLBI measurements of the Phobos Spacecraft's approach to Mars (Hildebrand *et al.*, 1994),
- • VLBI measurements of the Magellan Spacecraft orbiting Venus (Folkner, 1992, 1993, 1994a, 1994b),
- • VLBI, doppler, and range measurements from the Ulysses Spacecraft's encounter with Jupiter (Folkner and McElrath, 1993),
- • a range measurement from the Phobos Spacecraft's approach to Mars (Berthias, 1990), and
- • re-processing of the Voyager 1 tracking files from the Jupiter encounter (Folkner and Haw, 1995).

Figures 5a–5h show plots of the residuals of the VLBI observations of the Magellan (Figures 5a–5e), Phobos (Figures 5f–5g) and Ulysses (Figure 5h) Spacecraft. The residuals are plotted in right ascension and declination and are surrounded by their *a priori* one-sigma uncertainty ellipsoids. As can be seen, only one (5b) has an error at all larger than 1 sigma. The shapes of the ellipsoids show that these VLBI observations have strength almost entirely in one dimension: on a line pointing about midway between the r.a. and dec. directions for the Goldstone-Canberra observations and pointing almost entirely in the r.a. direction for the Goldstone-Madrid observations. The widths of the ellipsoids, one to a few milliarcseconds, imply accuracies of 1 to 2 kilometers for the Venus and Mars observations and less than 10 km for the Ulysses observation at Jupiter.

Lunar Laser Ranging Data

The lunar laser ranging (LLR) data set consists of 9555 normal points from 1970 to 1995. The ranges are from five sites at three separate observatories (McDonald, Haleakala, and CERGA) on the earth to four sites (Apollo 11, 14, 15 and Lunakhod 2) on the moon. The residuals are plotted in Figure 6. The last several years of data can be fit with 3 cm rms scatter.

Compared to the data used for DE 200, the present data set is of longer span and, for recent ranges, much higher accuracy. Important precession periods in the motion of the moon are 6.0 yr (argument of perigee), 8.9 yr (longitude of perigee), and 18.6 yr (node). These periods are significant for determining different parameters, thus implying that long spans of accurate data are important. For example, the longest period governs the determination of the lunar orbit plane orientation.

Jupiter Residuals: Inconsistent Data

As mentioned above and as discussed in Standish (1995), the DE403 Jupiter ephemeris represents a compromise between inconsistent observations: "the orbital plane implied by the optical (FK5-based) observations disagrees with that implied by the IERS-based observations. The difference is about 0."2." The observational data for Jupiter which are not based upon the optical (FK5) reference system are listed in Table III along with the associated residuals. The consistency of the five range observations is exceptional. The right ascension and declination observations, however, are less than satisfying. The Voyager 1 residuals are about twice their *a priori* standard deviations. The residuals are plotted in Figures 7a and 7b along with the means of the optical

observations taken over each opposition of Jupiter. The stars represent the La Palma observations; triangles, Washington 6-inch transit; circles, Herstmonceux. The large squares, left-to-right, represent the Voyager 1, VLA, and Ulysses residuals, respectively. The right ascension residuals are reasonable, but the optical residuals in declination show an obvious negative bias while the residual from Voyager 1 is highly positive. The reason for this inconsistency is unknown. The residuals are tentatively attributed to biases for the optical observatories and an optical-IERS frame-tie. The numerical values from the solution, (+0.″00, −0.″02) for Herstmonceux, (+0.″01, −0.″06) for La Palma, and (−0.″03, −0.″06) for Washington, and 206265 $\mathbf{A}^T = [-0.''05, -0.''03, -0.''00]$ were *not* applied in Figures 7a and b. They must not be construed as an estimate of the true FK5-IERS frame-tie. Eventually, more will be known after VLBI observations are taken of the Galileo spacecraft in orbit about Jupiter, starting in 1996.

IV. DYNAMICAL MODELING

The basic part of the equations of motion for numerically integrating the ephemerides is the same as that described by Newhall *et al.* (1983). A few refinements have become necessary to accommodate the more recent LLR data (2–3 cm accuracy) and the Viking Lander ranging data, (2–3 m accuracy). The following are the significant modifications:

- • changes to the modeling of the lunar librations,
- • splitting of the tidal acceleration of the moon into contributions from diurnal and semidiurnal tides, and
- • the addition of the perturbations from three main taxonomic classes of asteroids.

Lunar Modeling

Since DE 200, many improvements have been made to the computation of lunar ranges and fits of lunar-related parameters. The set of solution parameters includes orbits of moon and earth, physical librations, observatory and reflector coordinates, lunar gravity harmonics and moment of inertia combinations, lunar Love numbers and rotational dissipation, GM of earth+moon, precession and nutation of the earth, earth rotation corrections (mainly to the earlier data span) and drifts, and tidal acceleration parameters. Plate motion is imposed on the stations. To improve compatibility with the planetary fits, partials are carried for the AU, earth/moon mass ratio, and planetary masses and orbits.

It is obvious that the LLR data determine the lunar orbit. In addition, the LLR data dominate the determination of the orientation between the equator and ecliptic planes. Since the IERS celestial coordinates are not aligned with the J2000 equator it is necessary to solve for the offset of the equator from the zero-declination plane of the IERS system (or equivalently, to solve for the offset of the rotation pole from the IERS north pole). The precession and obliquity rates have been adopted, the ecliptic plane is constrained, and the offsets are solved for. The offsets were treated as constant corrections to the two nutation components, which is an approximation. With T in centuries from J2000,

$\Delta\epsilon = -0.''00399 - 0.''024\ T+$ periodic nutation corrections, and

$\sin\epsilon\Delta y = -0.''01536 - 0.''1193\ T+$ periodic nutation corrections.

The periodic nutation corrections are adopted improvements in the nutations plus a solution for 18.6 yr terms using the constraints of Williams et al. (1991). The LLR data also contribute to the determination of the sidereal mean motion of the earth and determine the difference between the orbital longitudes of the geocentric moon and sun.

Tidal acceleration of the moon comes mainly from the ocean tides, but roughly 1% comes from dissipation in the moon. The present model for the orbit integration computes separate contributions from diurnal and semidiurnal earth tides. There are diurnal and semidiurnal tidal parameters

(time delays) determined in the ephemeris adjustments. The tidal acceleration is computed to be -25".8/cty^2 for the sum of the one lunar and two earth contributions.

Asteroid Perturbations

There are quite a few asteroids whose perturbations produce a non-negligible effect upon the orbits of the major planets. For the JPL ephemerides, these are handled in two different ways.

The "Big 3": Ceres, Pallas, and Vesta, are handled individually; they are assumed to follow periodic Keplerian orbits, described by chebychev polynomials:

- • osculating elements are first transformed into mean elements (Williams, 1989);
- • from the mean elements, positions for each asteroid are computed throughout one of its periods;
- • these positions are fit with chebychev polynomials, to be interpolated later during the integration;
- • the interpolated positions are combined with a pre-assigned mass to compute the force which is applied to every planet.
- • Corrections to the mass of each of the three asteroids may be solved for.

The 297 next most important asteroids are handled in a different manner:

- • the 297 asteroids are grouped according to approximate taxonomic class: C, S, or M;
- • osculating elements are transformed into mean elements;
- • the volume of each asteroid is computed from its estimated diameter, and a density is assigned according to its taxonomic class;
- • vectors of the forces upon Mars, the earth and the moon are computed for each asteroid and summed over all of the asteroids in the class;
- • these sums are stored in a file for every other day throughout the entire interval over which the ephemeris is to be integrated;
- • the forces are interpolated from the file and used in the equations of motion during the integration.
- • Corrections to the density of each of the three classes may be solved for.

It should be noted in both cases, that the asteroids' contributions to the location of the center of mass of the solar system are accounted for.

The masses of the asteroids, Ceres, Pallas and Vesta for DE403 are seen to be 7% , 25% and 11% lower, respectively, than those estimated by Standish and Hellings (1989). Interestingly, these newer results for Pallas and Vesta are quite close to the original values by Schubart (1975); however, the uncertainties involved, approximately the sizes of the changes themselves, show this to be probably coincidental.

In a series of preliminary experiments, it was seen that determinations of the densities of the M-class of asteroids produced untrustworthy results; consequently, that value was adopted as 5.0 gm/cm^3 and not solved-for. The determined values of the densities of the C- and S-classes, 1.80 and 2.40, must be regarded as quite tentative; their influences upon the motions of the earth and Mars are barely detectable. Other unmodeled signatures in the observations could easily give false

results for these; e.g., just a 10% bias in the asteroids' diameters would change these result by 30% .

A file of the asteroids whose perturbations were modeled in the ephemerides is maintained by the authors.

V. COMPARISON OF DE403/LE403 WITH DE200/LE200

Figures 8a-8o show comparisons of geocentric coordinates of the inner planets and moon between DE403/LE403 and DE200/LE200. Over the full interval of nearly six centuries, the mean motion differences for the inner four planets are apparent. Presumably, most of the error is due to DE200: improvements to the ephemerides since DE200 have come from more extensive sets of observational data, enhanced modeling of the asteroids' perturbations, improved values of the outer planet masses, refined modeling of the surfaces of Mercury and Venus, etc. The expanding envelopes for the differences in distance simply reflect the growing longitude offsets coupled with non-zero eccentricities and changing distances.

For the outer planets, Figures 9a-9o show that the agreement over the present century is within a few tenths of an arcsecond. The large differences in the other centuries show the inherent uncertainty of extrapolating those orbits beyond the observational data coverage.

Problems with DE118 and DE200

For the moon, it is now quite apparent that DE118 (and therefore, DE200) contains a significant error in the lunar longitude for the years prior to 1750. The integration of DE118 was performed in a number of separate computer runs, where it was necessary to restart the integration process each time from where the previous run had ended. The backward integrations covered the time-spans, 1969 to 1900, 1900–1850, 1850–1800, 1800–1750, 1750–1664, and 1664–1600; the forward pieces covered 1969–1990, 1990–2050, 2050–2169, and 2169 to 2200. Back when these runs were made, the restart process was not automatic: there was a major error, affecting all planets, committed at the restart in 2169 which has long been known; also, there was a minor error made in the restart at 1750 which has only recently come to light. This latter error affects mainly the lunar longitude, causing a run-off which reaches nearly 40 arcseconds by the year 1600. As a result, DE118 and DE200 are strictly valid over only the interval 1750 to 2169. The geocentric differences for the moon are shown in Figures 8m-8o. Over the valid interval, the difference of about -0."9/cty^2 for the deceleration in longitude can be seen; before 1750, the run-off dominates.

VI. CONSTANTS, INITIAL CONDITIONS, ETC.

Given in Table IV are the dynamical constants used in DE403/LE403; the initial conditions at the starting epoch of the integration, JED 2440400.5 (28 June 1969), are given in Table V.

Availability of DE403

Sections of DE403 are now available from the anonymous ftp site: "navigator.jpl.nasa.gov" [128.149.23.82].

For a "navio" version (in-house JPL format), the following "navio" and "nioftp" versions are available, covering 1980–2010:

"navigator:/ephem/navio/de403s" and "navigator:/ephem/navio/de403s.ftp"

For other time-spans, contact F A McCreary (faith@viviane.jpl) or E M Standish (ems@smyles.jpl).

An outside user is advised to first get and read the file, "navigator:/ephem/export/READ.ME"; it should answer most questions about retrieving and using the JPL ephemerides.

DE404/LE404, the New "JPL Long Ephemeris"

As of this writing, DE403/LE403 has been integrated over the same interval as that covered by

DE102, the previous "JPL Long Ephemeris": 1410 BC to 3000 AD. It will soon be extended further, probably back to 3000 BC. At that time, it will be condensed and re-numbered DE404/LE404. The condensation involves three parts:

- 1. The elimination of the nutations from the file. Nutations may be obtained exactly from a formula.
- 2. The lunar librations are removed from the file. A second file containing only the librations will be made available.
- 3. The accuracy of the interpolating polynomials will be lessened (though interpolation on the 64-day mesh points will remain exact). For DE404/LE404, the interpolating accuracy will be no worse than 25 meters for all planets and no worse than 1 meter for the moon – adequate for nearly any application except for the processing of the most accurate observations.

DE404/LE404 will occupy only 3.3 megabytes per century as opposed to the full DE403/LE403 which requires 9.2 megabytes per century. For the full expanse, 3000 BC to 3000 AD, DE404/LE404 will require only 200 megabytes.

VII. CONCLUSION

It is believed that DE403/LE403 represent substantial improvements over any previous planetary or lunar ephemerides. Certainly, though, they are not perfect; extrapolation will always show deterioration. Even now, continued improvements in modeling are being incorporated, while newer and more accurate data types will offer even higher accuracy in the future. For the present, however, it is felt that DE403/LE403 represent state-of-the-art planetary and lunar positions.

VIII. REFERENCES

Berge,G.L., Muhleman,D.O., and Linfield,R.P.: 1988, "Very Large Array Observations of Uranus at 2.0 cm", *Astron. J.*,**96**, #1, 388–395.

Berthias, J.P.: 1990, "Analysis of the Phobos 2 radiometric data set", JPL IOM 314.6-1129.

Borderies, N.: 1980, "La Rotation de Mars: Théorie Analytique Analyse d'observations de l'expérience Viking", thesis, Université Paul Sabatier de Toulouse.

Charlot, P., Sovers, O.J., Williams, J.G., and Newhall, X X: 1995, "Precession and nutation from joint analysis of radio interferometric and lunar laser ranging observations",*Astron. J.*, **109**, 418–427.

Christensen, E.J.: 1975, "Martian Topography Derived from Occultation, Radar, Spectral, and Optical Measurements", *J. Geophys. Res.*, **80**, # 20, 2909–2913.

Folkner, W.M.: 1992, "Preliminary results from VLBI measurement of Venus on September 12, 1990", JPL IOM 335.1-92-25.

Folkner, W.M.: 1993, "Results from VLBI measurement of Venus on March 29, 1992", JPL IOM 335.1-93-22.

Folkner, W.M.: 1994a, "Results from VLBI measurements of Venus on December 22 and December 23, 1991", JPL IOM 335.1-94-006.

Folkner, W.M.: 1994b, "Results from VLBI measurement of Venus on April 1, 1994", JPL IOM 335.1-94-014.

Folkner, W.M.: 1995, private communication.

Folkner, W.M. and Haw, R.J.: 1995, "Determination of the Position of Jupiter from Radio Metric Tracking of Voyager 1", submitted for publication in JPL TDA Progress Report.

Folkner, W.M. and McElrath, T.P.: 1993, "Determination of Radio-Frame Position for Earth and Jupiter from Ulysses Encounter Tracking", AAS/AIAA Paper AAS 93–167.

Folkner, W.M., Charlot, P., Finger, M.H., Williams, J.G., Sovers, O.J., Newhall, X X, and Standish, E.M.: 1993, "Determination of the extragalactic frame tie from joint analysis of radio interferometric and lunar laser ranging measurements", *Astron. Astrophys.*, **287**, 279–289.

Fricke, W.: 1971, "A Rediscussion of Newcomb's Determination of Precession", *Astron. Astrophys.* **13**, 298–308.

Fricke, W.: 1982, "Determination of the Equinox and Equator of the FK5", *Astron. Astrophys.* **107**, L13–L16.

Gemmo, A.G. and Barbieri, C.: 1993, "Astrometry of the Planet Pluto in the Years 1969–1989", submitted to *Icarus*.

Hildebrand, C.E., Iijima, B.A., Kroger, P.M., and Folkner, W.M.: 1994, "Radio-Planetary Frame Tie From Phobos-2 VLBI Data", JPL TDA Progress Report 42-119, 46-82.

Lieske, J.H., Lederle, T., Fricke, W., and Morando, B.: 1977, "Expressions for the Precession Quantities Based upon the IAU (1976) System of Astronomical Constants", *Astron. Astrophys.*, **58**, 1–16.

Lyttleton, R.A., Cain, D.L. and Liu, A.S.: 1979,"Nutation of Mars", JPL Publication 79–85.

Monet, A.B.: 1994, private communication.

Morrison, L.V., Buontempo, M.E., Fabricius, C., and Helmer, L.: 1992, "First meridian circle observations of Pluto", *Astron. Astrophys.*, **262**, 347-349.

Muhleman, D.O., Berge, G.L., Rudy, D.J., Niell, A.E., Linfield, R.P. and Standish, E.M.: 1985, "Precise Position Measurements of Jupiter, Saturn and Uranus Systems with the Very Large Array", *Cel. Mech.*, **37**, 329–337.

Muhleman, D.O., Berge, G.L. and Rudy, D.: 1986, "Precise VLA Positions and Flux-Density Measurements of the Jupiter System", *Astron. J.*,**92**, #6, 1428–1435.

Muhleman, D.O., Berge, G.L. and Jones, D.:1988, "VLA Observations of Neptune and the Mass of Triton", informal report, CalTech.

Newhall, X X, Standish, E.M. and Williams, J.G.: 1983, "DE102: a numerically integrated ephemeris of the Moon and planets spanning forty-four centuries", *Astron. Astrophys.*, **125**, 150–167.

Nicholson, P.D.: 1992, private communication.

Pettengill, G.H., Eliason, E., Ford, P.G., Loriot, G.B., Masursky, H., and McGill, G.E.: 1980, "Pioneer Venus Radar Results: Altimetry and Surface Properties", *J. Geophys. Res.*, **85**, A13, 8261–8270; table of values transmitted to the authors via W L Sjogren.

Reasenberg, R.D. and King, R.W.: 1979, "The Rotation of Mars", *J. Geophys. Res.*, **84**, B11, 6231–6240.

Schubart, J.: 1975, "The mass of Pallas", *Astron. Astrophys.*, **39**, 147–148.

Schwan, H. : 1977, "Development and Testing of a Method to Derive an Instrumental System of Positions and Proper Motions of Stars", Veröffentlichungen # 27, Astronomisches Rechen-Institut, Heidelberg.

Souchay, J., Feissel, M., Bizouard, C., Capitaine, N., and Bougeard, M.: 1995, "Precession and nutation for a non-rigid earth model: comparison between theory and VLBI observations", *Astron. Astrophys.*, in press.

Standish, E.M., Keesey, M.S.W. and Newhall, X X : 1976, "JPL Development Ephemeris Number 96", JPL Tech. Rep., 32-1603, Pasadena.

Standish, E.M.: 1982, "Orientation of the JPL Ephemerides, DE200/LE200, to the Dynamical Equinox of J2000", *Astron. Astrophys.*, **114**, 297-302.

Standish, E.M.: 1985, "Planetary and Lunar Ephemerides, DE125/LE125", JPL IOM 314.6-591.

Standish, E.M.: 1990, "The observational basis for JPL's DE200, the planetary ephemerides of the Astronomical Almanac", *Astron. Astrophys.*, **233**, # 1, 252-271.

Standish, E.M.: 1995, "DE403/LE403: Announcement",JPL IOM 314.10-124.

Standish, E.M. and Folkner, W.M.: 1995, "DE400/LE400 and DE140/LE140: Delivery and Covariances", JPL IOM 314.10-109.

Standish, E.M., Newhall, X X, Williams, J.G. and Folkner, W.F.: 1995, "JPL Planetary and Lunar Ephemerides, DE402/LE402", JPL IOM 314.10-117.

Standish, E.M. and Hellings, R.W.: 1989, "A Determination of the Masses of Ceres, Pallas and Vesta from their Perturbations upon the Orbit of Mars", *Icarus*, **80**, 326-333.

Stone, R.C.: 1995, private communication.

Williams, J.G.: 1989, "Harmonic Analysis", *BAAS*, **21**, # 3, 1009.

Williams, J.G.: 1994, "Contributions to the Earth's obliquity rate, precession, and nutation", *Astron. J.*, **108**, 711

Williams, J. G., Newhall, X X, and Dickey, J. O.; 1991, "Luni-solar Precession: Determination from Lunar Laser Ranges", *Astron. Astrophys.*, **241**, L9-L12

Williams, J.G., Newhall, X X, and Dickey, J.O.: 1994, "Determination of precession and nutation from lunar laser ranging analysis", *IAU JD19*, to appear in *Highlights of Astronomy.*

Distribution

announced to Section 312 via e-mail

Table I. Observational data fit by DE403/LE403. The columns contain the source, the time coverage, the planets measured, the components measured, the *a priori* uncertainties of a measurement, the number of observations and the group totals.

OPTICAL MERIDIAN TRANSITS						
Washington	1911–1994	Sun, ..., Nep	ra,dec	1".0/0".5	14234	
Herstmonceux	1957–1982	Sun, ..., Nep	ra,dec	1".0/0".5	2855	17089
Bordeaux	1985–1993	Sat, Ura, Nep	ra,dec	0".25	850	
PHOTOELECTRIC MERIDIAN TRANSITS						
La Palma	1984–1993	Mar, ..., Plu	ra,dec	0".25	4751	
Tokyo	1986–1988	Mar, ..., Nep	ra,dec	0".5	502	
Flagstaff - USNO	1995	Plu	ra,dec	0".1	20	6123
Bordeaux	1996	Plu	ra,dec	0".1	850	
ASTROLABE						
Quito	1969	Sat	ra,dec	0".3–1".6	1	
Algiers	1969–1973	Mar,Sat			48	
SanFernando	1970–1978	Mar,Jup,Sat			338	
Besançon	1971–1973	Sat			44	
Paris	1971–1978	Mar,Sat			146	
CERGA	1972–1981	Mar,Jup,Sat			202	
Santiago	1975–1985	Ura			284	1063
PHOTOGRAPHIC ASTROMETRY OF PLUTO						
(Pre-disc)	1914–1927	Pluto	ra,dec	0".5	28	
Lowell	1930–1951				620	
Yerkes-McD	1930–1953				310	
(Nrml pts.)	1930–1958				66	
MacDonald	1949–1953				56	
Yerkes	1962–1963				42	
Palomar	1963–1965				8	
Dyer	1964–1981				44	
Bordeaux	1967				24	
Asiago	1969–1978				350	
Torino	1973–1982				74	
Copenhagen	1975–1978				150	
Flagstaff	1980–1994				16	
Lick	1980–1985				56	
La Silla	1988–1989				58	1902
OCCULTATION TIMINGS						
Uranus rings	1977–1983	Ura	ra,dec	0".14	14	
Neptune disk	1968–1985	Nep	ra,dec	0".27	18	32

RADIO ASTROMETRY OF THERMAL EMISSION						
VLA	1987	Jup, ..., Nep	ra,dec	0.″03–0.″1	10	10
RADAR RANGING						
Arecibo	1967–1982	Mer,Ven	range	10 km	469	
Haystack	1966–1971	Mer,Ven		1.5	433	
Millstone	1964–1967	Ven		10	17	
Goldstone13	1964–1970	Ven		1.5	24	
Gldstn 13–14	1970–1977	Mer,Ven		1.5	23	
Goldstone14	1970–1993	Mer,Ven		1.5	365	1331
SPACECRAFT MEASUREMENTS						
Mariner 9	1971–1972	Mars	range	35–120 m	629	
Pioneer 10	1973	Jupiter	range	3 km	1	
Pioneer 11	1974			12 km	1	
Viking Lander	1976–1980	Mars	range	7 m	1018	
	1980–1981			12 m	264	
Voyager 1 OD	1979	Jupiter	r.a., dec.	0.″01,0.″05	2	
			range	3 km	1	
Voyager 2 OD	1979		range	3 km	1	
Phobos OD	1989	Mars	range	0.5 km	1	
Phobos VLBI	1989	Mars	r.a., dec.	0.″01–0.″1	4	
Ulysses VLBI & OD	1992	Jupiter	r.a., dec.	0.″003,0.″006	2	
			range	3 km	1	
Magellan VLBI	1990–1994	Venus	r.a., dec.	0.″003–0.″1	10	1935
LUNAR LASER RANGING						
McDnld 107″	1970–1976	Moon	range	20–30 cm	2045	
	1977–1982			15	1233	
	1983–1985			20	173	
McDnld LRS (old site)	1985–1988			5–10	275	
McDnld LRS (new site)	1988–1995			2–3	702	
CERGA	1984–1987			8–10	1217	
	1988–1989			5–7	574	
	1990–1991			4–5	996	
	1992–1995			2–3	1646	
Haleakala	1984–1988			8–10	558	
	1989–1990			3–5	136	9555
FRAME-TIE DETERMINATION						
IERS FRAME-TIE	1988	Earth	$\hat{\mathbf{r}}_\oplus$, $\hat{\mathbf{h}}_\oplus$	0.″003	12	12
CONSTRAINTS AND NOMINAL VALUES						
Lunar Parameters		Moon			5	5
TOTAL						39057

Table II. Parameters from the Viking Lander Observations. The estimated parameters are shown with their formal (i.e., optimistic) uncertainties; the other parameters were adopted.

Prime meridian	V	133.°69448	—
Spin-rate	$\dot{V}$	350.°89198475/day	± 0.°00000014/day
Inclination of equator to orbit	I_q	25.°1931	± 0.°0005
Rate of Inclination of equator to orbit	$\dot{I}_q$	0.°00000057/day	± 0.°00000007/day
Node of equator upon orbit	Ω_q	35.°5100	± 0.°0011
Rate of Node of equator upon orbit	$\dot{\Omega}_q$	0.°0000123/day	± 0.°0000001/day
Inclination of orbit to ecliptic	I	1.°85	—
Rate of Inclination of orbit to ecliptic	$\dot{I}$	-0.°0/day	—
Node of orbit upon ecliptic	Ω	49.°5448	—
Rate of Node of orbit upon ecliptic	$\dot{\Omega}$	-0.°000018/day	—
Obliquity of ecliptic	ϵ	23.°439281	—
Rate of Obliquity of ecliptic	$\dot{\epsilon}$	-0.°000000355/day	—
Spin-axis distance	u_1	3136.516 km	± 0.001 km
Z-height	v_1	1284.484 km	± 0.012 km
Longitude	λ_1	311.°7359	± 0.°0011
Spin-axis distance	u_2	2277.378 km	± 0.002 km
Z-height	v_2	2500.094 km	± 0.012 km
Longitude	λ_2	133.°9676	± 0.°0011

Table III. Residuals of Jupiter for DE403/LE403 in right ascension, declination, and range.

Pioneer 10	4 Dec 1973			-1.0 km $\pm$ 3.0 km
Pioneer 11	3 Dec 1974			-2.4 km $\pm$ 12.0 km
Voyager 1 OD	5 Mar 1979	$+0.''035$ $\pm$ $0.''020$	$+0.''113$ $\pm$ $0.''050$	-2.1 km $\pm$ 3.0 km
Voyager 2 OD	9 Jul 1979			-3.1 km $\pm$ 3.0 km
VLA	Apr/May 1983	$-0.''015$ $\pm$ $0.''030$	$-0.''036$ $\pm$ $0.''060$	
Ulysses VLBI OD	8 Feb 1992	$-0.''003$ $\pm$ $0.''003$	$+0.''005$ $\pm$ $0.''006$	$+0.2$ km $\pm$ 3.0 km

Table IV. Primary constants for DE403/LE403

JED SPAN : 2305200.50 (1599 APR 29) to 2524400.50 (2199 JUN 22)

AU	149597870.691	[km/au]
CLIGHT	299792.458	[km/sec]
EMRAT	81.300585	[GM(earth)/GM(moon)]

	[au^3/day^2]	[GM$_{\rm Sun}$ /GM$_{\rm i}$]		[km^3/sec^2]
GM1	$0.4912547451450812...\times10^{-10}$	6023600	.	22032.080...
GM2	$0.7243452486162703...\times10^{-09}$	408523	.71	324858.599...
GM3	$0.8887692450565006...\times10^{-09}$	332946	.048630...	398600.436...
GM4	$0.9549535105779258...\times10^{-10}$	3098708	.	42828.314...
GM5	$0.2825345909524226...\times10^{-06}$	1047	.3486	126712767.863...
GM6	$0.8459715185680659...\times10^{-07}$	3497	.898	37940626.063...
GM7	$0.1292024916781969...\times10^{-07}$	22902	.98	5794549.007...
GM8	$0.1524358900784276...\times10^{-07}$	19412	.24	6836534.064...
GM9	$0.2188699765425970...\times10^{-11}$	135200000	.	981.601...
GMS	0.01720209895^2	1	.	132712440023.310...
GMM	$0.1093189237268710...\times10^{-10}$	27068708	.527072...	4902.799...
GMB	$0.8997011374291877...\times10^{-09}$	328900	.560392...	403503.235...

	[au^3/day^2]	[GM$_{\rm i}$ /GM$_{\rm Sun}$]		[km^3/sec^2]
MA0001	$0.1373032646445143...\times10^{-12}$	4.64	$\times10^{-10}$	61.579...
MA0002	$0.3107078186998706...\times10^{-13}$	1.05	$\times10^{-10}$	13.935...
MA0004	$0.3965223591026921...\times10^{-13}$	1.34	$\times10^{-10}$	17.783...

Table V. DE403/LE403 positions and velocities at the integration epoch. Heliocentric planets, geocentric moon, solar-system-barycentric sun at JED 2440400.5 (June 28, 1969), in au and au/day.

Mercury	0.3572602074480422	−0.0915490527316210	−0.0859810319208761
	0.0033678460665285	0.0248893425409419	0.0129440718036641
Venus	0.6082494267602045	−0.3491324543998684	−0.1955443458956939
	0.0109524203859526	0.0156125066152813	0.0063288762775591
EM-Bary	0.1160148927753046	−0.9266055561260659	−0.4018062765483065
	0.0168116200832907	0.0017431314053870	0.0007559737321629
Mars	−0.1146886056013058	−1.3283665295535771	−0.6061551879562506
	0.0144820048109846	0.0002372852487673	−0.0002837498575510
Jupiter	−5.3842094067801511	−0.8312470356991036	−0.2250958486572985
	0.0010923631195394	−0.0065232933425626	−0.0028230144378031
Saturn	7.8898916979858358	4.5957078575699830	1.5584322051523174
	−0.0032172026168370	0.0043306325527844	0.0019264178272449
Uranus	−18.2698980946940850	−1.1627140690156066	−0.2503719383072875
	0.0002215404476082	−0.0037676538996767	−0.0016532444914441
Neptune	−16.0595376822070435	−23.9429495784517492	−9.4004295388809425
	0.0026431230271517	−0.0015034921971370	−0.0006812710717939
Pluto	−30.4878237352859180	−0.8732645031545428	8.9113111554337117
	0.0003225614206968	−0.0031487486744659	−0.0010801816958473
Moon	−0.0008081773574186	−0.0019946299933645	−0.0010872626574534
	0.0006010848150497	−0.0001674454694227	−0.0000855621455018
Sun	0.0045025071581463	0.0007670751005129	0.0002660580862096
	−0.0000003517482825	0.0000051776245516	0.0000022291038556

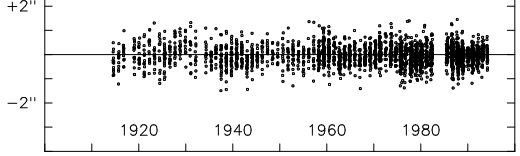

Fig. 1a. Transit residuals of Jupiter in right ascension.

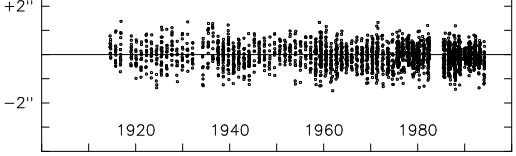

Fig. 1b. Transit residuals of Jupiter in declination.

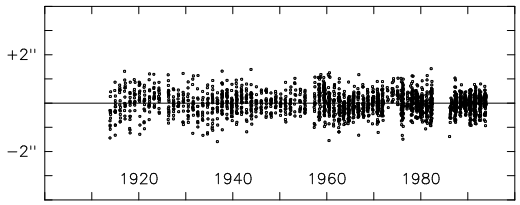

Fig. 1c. Transit residuals of Saturn in right ascension.

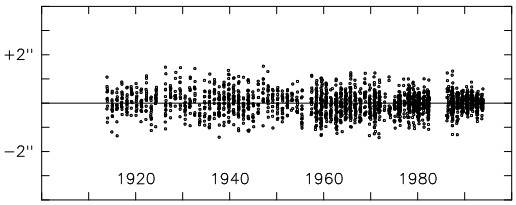

Fig. 1d. Transit residuals of Saturn in declination.

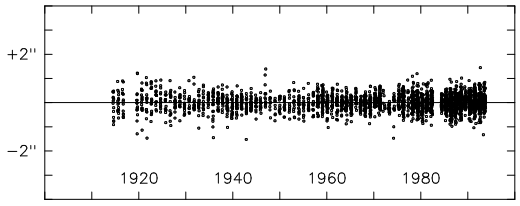

Fig. 1e. Transit residuals of Uranus in right ascension.

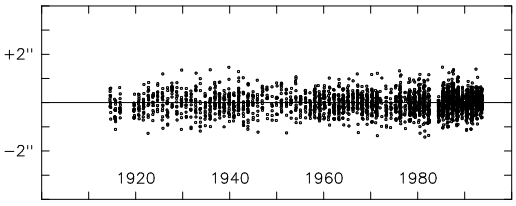

Fig. 1f. Transit residuals of Uranus in declination.

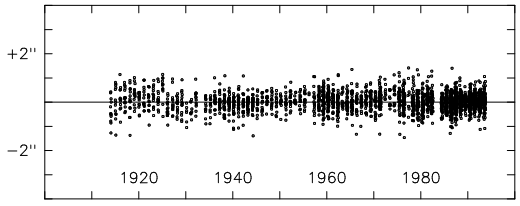

Fig. 1g. Transit residuals of Neptune in right ascension.

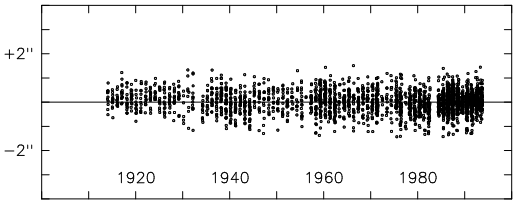

Fig. 1h. Transit residuals of Neptune in declination.

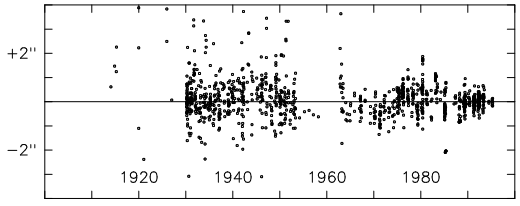

Fig. 1i. Transit and photographic residuals of Pluto in right ascension.

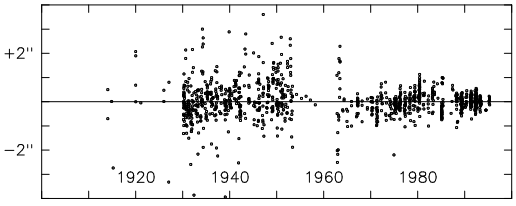

Fig. 1j. Transit and photographic residuals of Pluto in declination

Figure 1:

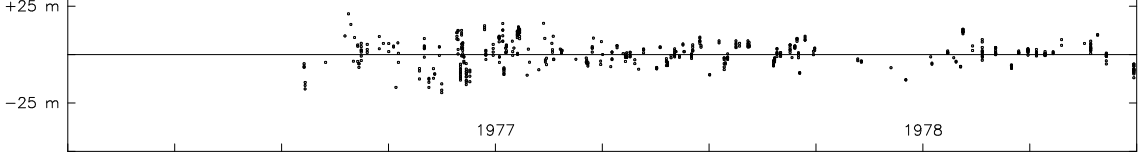

Fig.2a. Viking Lander Range Residuals, 1976.0 – 1978.5

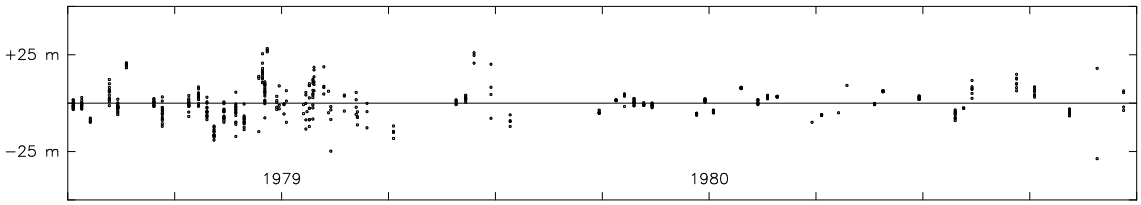

Fig.2b. Viking Lander Range Residuals, 1978.5 – 1981.0

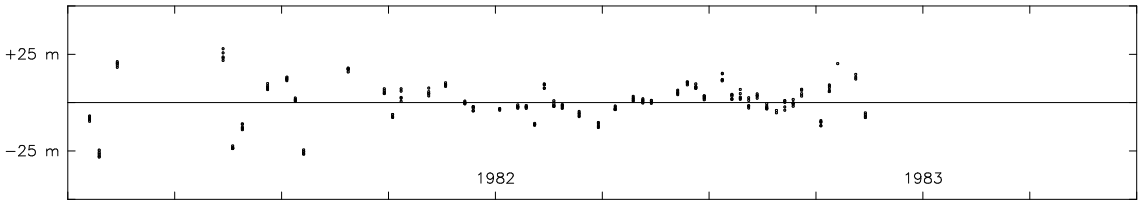

Fig.2c. Viking Lander Range Residuals, 1981.0 – 1983.5

Figure 2:

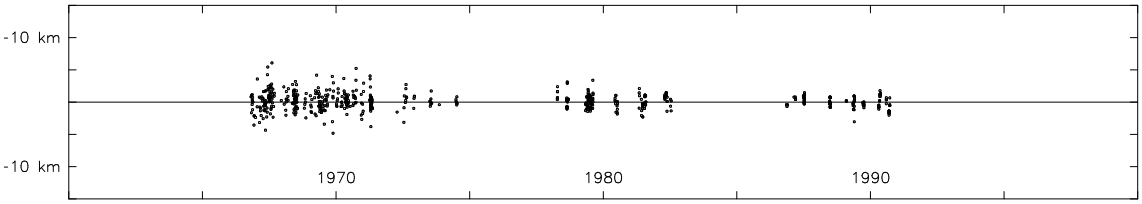

Fig.3a. Radar residuals of Mercury

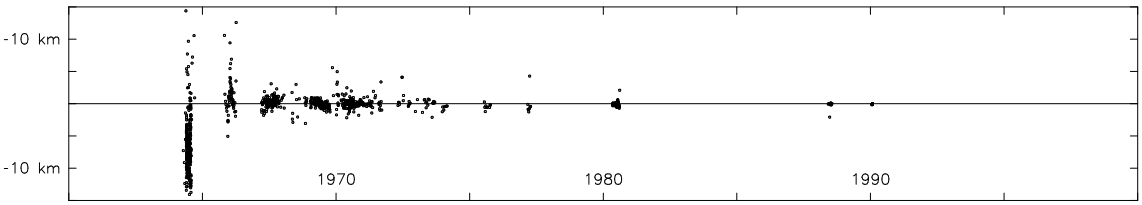

Fig.3b. Radar residuals of Venus

Figure 3:

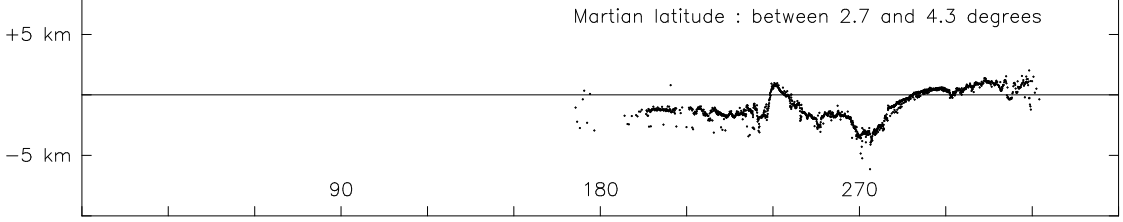

Fig.4a. 1975−1976 Mars radar residuals wrt the 6−mb surface

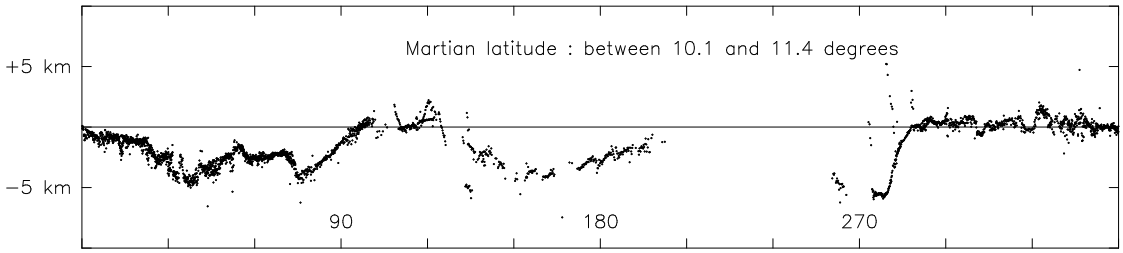

Fig.4b. 1978 Mars radar residuals wrt the 6−mb surface

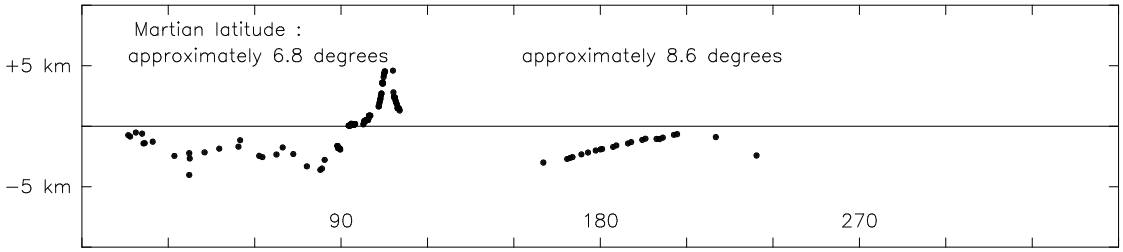

Fig.4c. 1992−1993 Mars radar residuals wrt the 6−mb surface

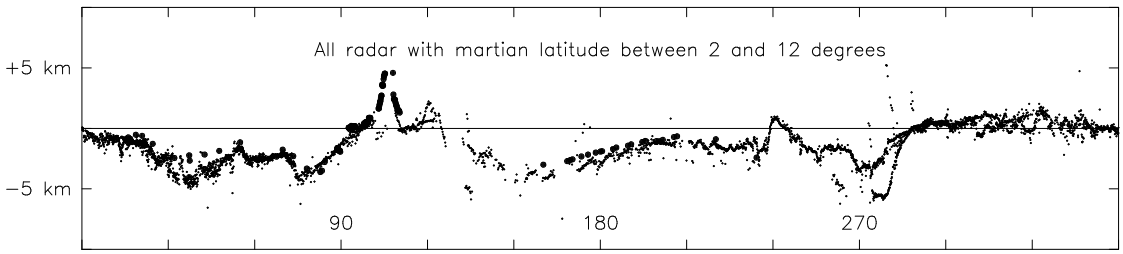

Fig.4d. Combined Mars radar residuals wrt the 6−mb surface

Figure 4:

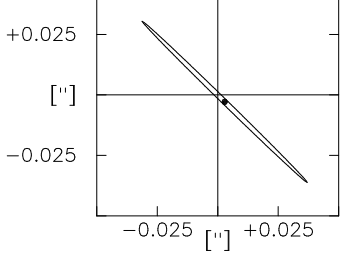

Fig.5a Magellan at Venus 1990 SEP 12

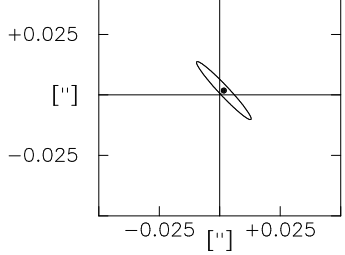

Fig.5b Magellan at Venus 1991 DEC 22

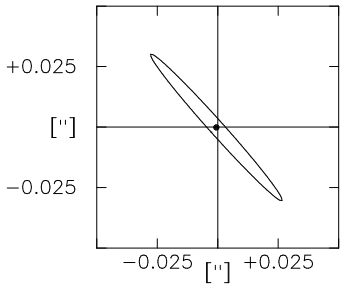

Fig.5c Magellan at Venus 1991 DEC 23

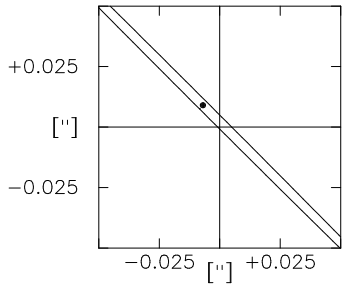

Fig.5d Magellan at Venus 1992 MAR 29

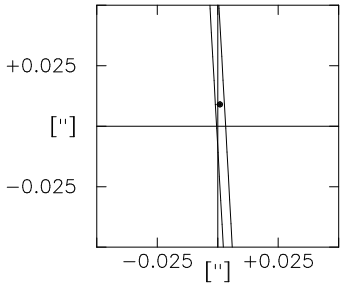

Fig.5e Magellan at Venus 1994 APR 01

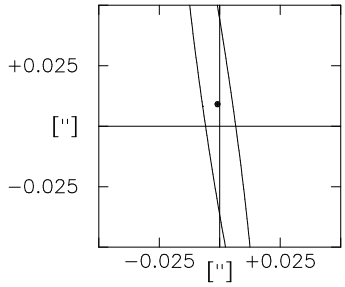

Fig.5f Phobos at Mars 1989 FEB 17

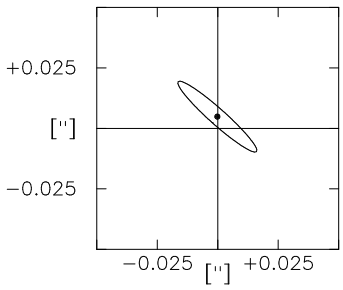

Fig.5g Phobos at Mars 1989 MAR 25

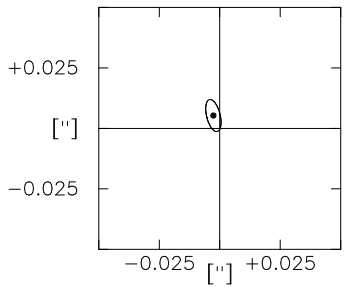

Fig.5h Ulysses at Jupiter 1992 FEB 08

Figure 5:

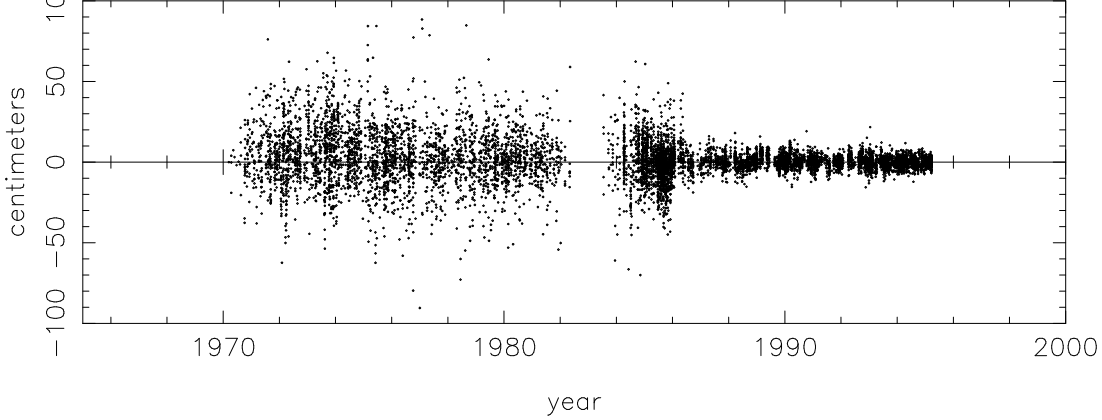

Figure 6:

Fig. 7a. DE403 Opposition Means of Jupiter in Right Ascension

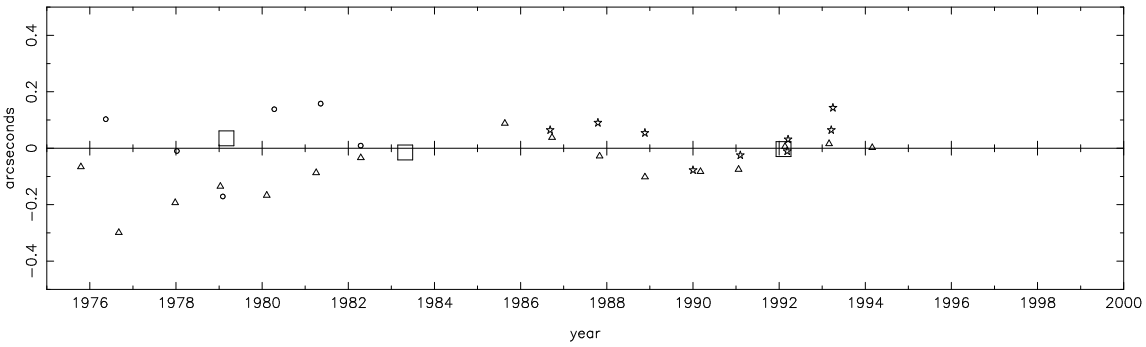

Fig. 7b. DE403 Opposition Means of Jupiter in Declination

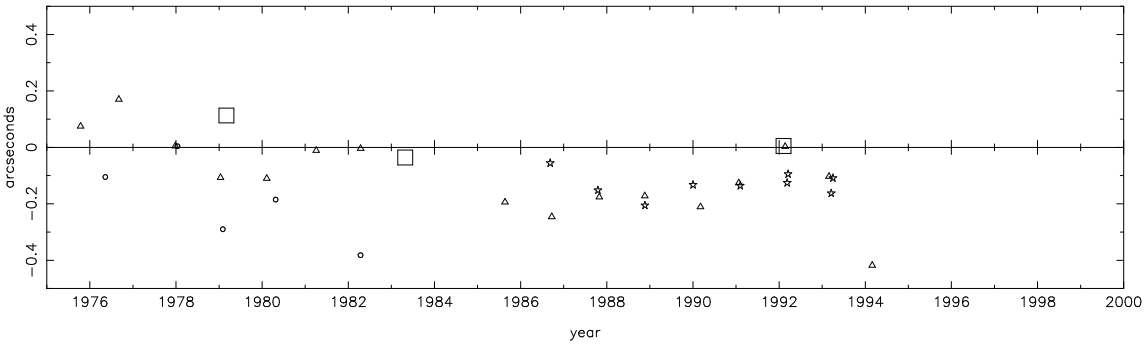

Figure 7:

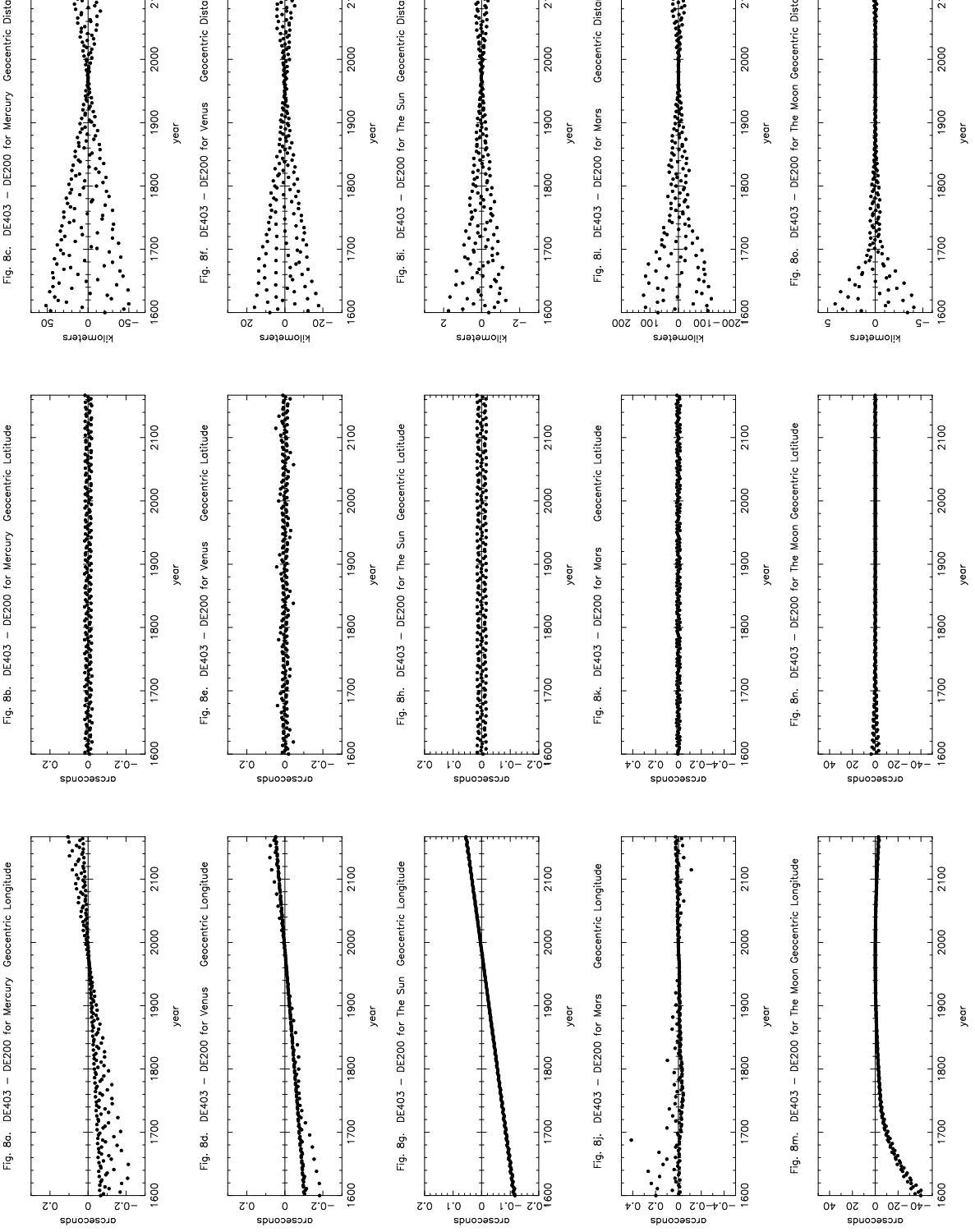
Fig. 8a. DE403 − DE200 for Mercury Geocentric Longitude
Fig. 8b. DE403 − DE200 for Mercury Geocentric Latitude
Fig. 8c. DE403 − DE200 for Mercury Geocentric Distance
Fig. 8d. DE403 − DE200 for Venus Geocentric Longitude
Fig. 8e. DE403 − DE200 for Venus Geocentric Latitude
Fig. 8f. DE403 − DE200 for Venus Geocentric Distance
Fig. 8g. DE403 − DE200 for The Sun Geocentric Longitude
Fig. 8h. DE403 − DE200 for The Sun Geocentric Latitude
Fig. 8i. DE403 − DE200 for The Sun Geocentric Distance
Fig. 8j. DE403 − DE200 for Mars Geocentric Longitude
Fig. 8k. DE403 − DE200 for Mars Geocentric Latitude
Fig. 8l. DE403 − DE200 for Mars Geocentric Distance
Fig. 8m. DE403 − DE200 for The Moon Geocentric Longitude
Fig. 8n. DE403 − DE200 for The Moon Geocentric Latitude
Fig. 8o. DE403 − DE200 for The Moon Geocentric Distance
arcseconds
kilometers
year
1600
1700
1800
1900
2000
2100

Figure 8:

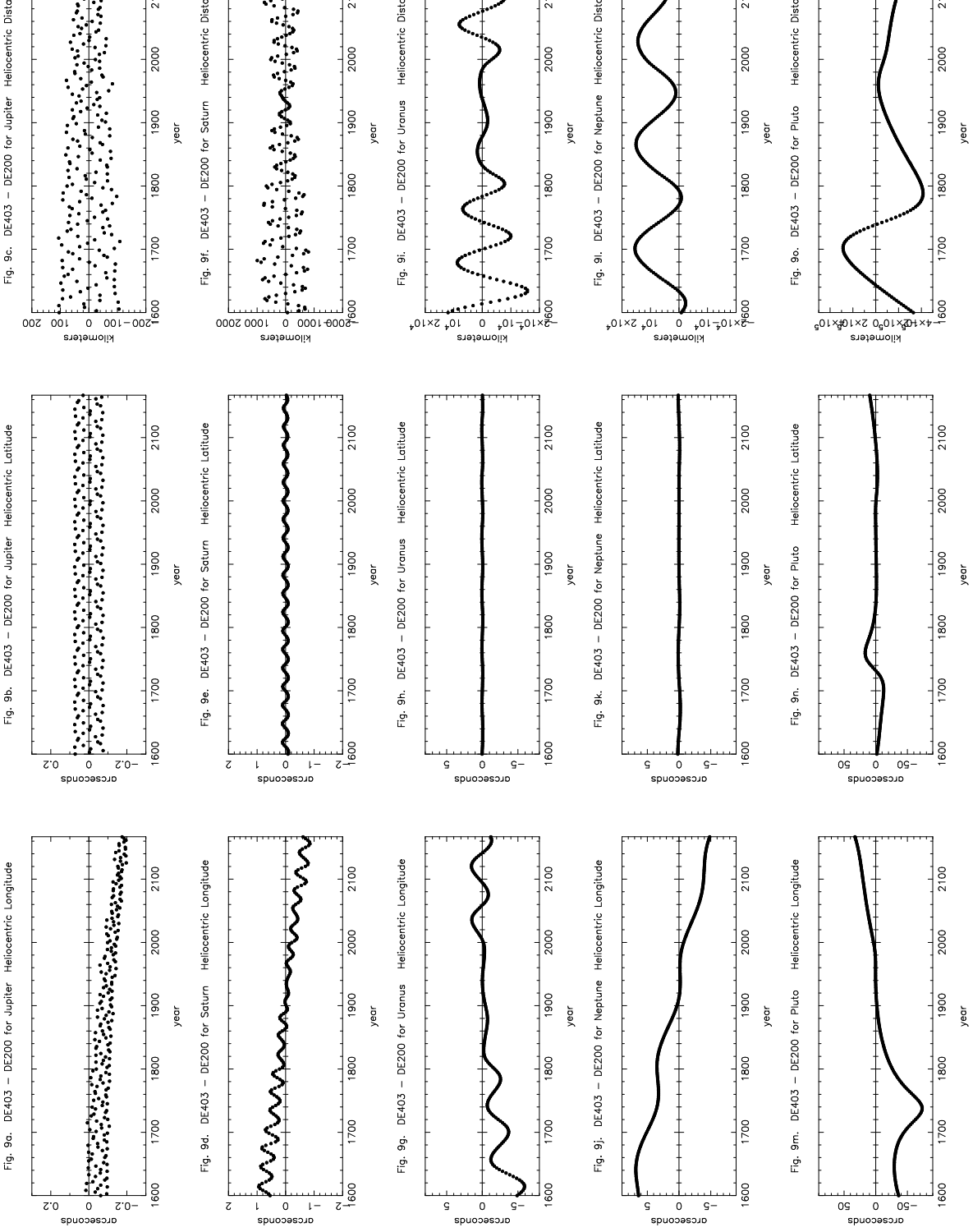
Fig. 9a. DE403 − DE200 for Jupiter Heliocentric Longitude
Fig. 9b. DE403 − DE200 for Jupiter Heliocentric Latitude
Fig. 9c. DE403 − DE200 for Jupiter Heliocentric Distance
Fig. 9d. DE403 − DE200 for Saturn Heliocentric Longitude
Fig. 9e. DE403 − DE200 for Saturn Heliocentric Latitude
Fig. 9f. DE403 − DE200 for Saturn Heliocentric Distance
Fig. 9g. DE403 − DE200 for Uranus Heliocentric Longitude
Fig. 9h. DE403 − DE200 for Uranus Heliocentric Latitude
Fig. 9i. DE403 − DE200 for Uranus Heliocentric Distance
Fig. 9j. DE403 − DE200 for Neptune Heliocentric Longitude
Fig. 9k. DE403 − DE200 for Neptune Heliocentric Latitude
Fig. 9l. DE403 − DE200 for Neptune Heliocentric Distance
Fig. 9m. DE403 − DE200 for Pluto Heliocentric Longitude
Fig. 9n. DE403 − DE200 for Pluto Heliocentric Latitude
Fig. 9o. DE403 − DE200 for Pluto Heliocentric Distance
arcseconds
kilometers
year
1600
1700
1800
1900
2000
2100

Figure 9: